ACS Catalysis

Research Article

pubs.acs.org/acscatalysis

Improved Low-Temperature CO Oxidation Performance of Pd Supported on La-Stabilized Alumina

Jason R. Gaudet,[†,§] Andrew de la Riva,[†] Eric J. Peterson,[†] Trudy Bolin,[‡] and Abhaya K. Datye*[,†]

[†]Department of Chemical & Nuclear Engineering & Center for Microengineered Materials, University of New Mexico, MSC 01 1120, Albuquerque, New Mexico 87131-0001, United States

[‡]Advanced Photon Source, Argonne National Laboratory, 9700 South Cass Avenue, Argonne, Illinois 60439, United States

Supporting Information

ABSTRACT: Simulated diesel oxidation catalysts (DOCs) consisting of 2.5% Pd were prepared on γ-Al_2O_3 and lanthana-stabilized γ-Al_2O_3; it was found that the La-containing catalyst had higher CO conversion and lower onset temperature for CO oxidation (~100 °C). Aberration-corrected STEM showed that the La–alumina support helped to stabilize Pd in smaller particles and clusters, increasing dispersion from 17 to 26%. The higher dispersion was responsible, in part, for the improved CO oxidation rate; at 140 °C, the turnover frequency (TOF) was improved from 0.0019 to 0.0095 s^{-1} with the addition of La. This TOF increase appears to be tied to facile redox behavior of the Pd/La–alumina catalyst, which was evident in the results of in situ X-ray absorption spectroscopy (XAS) and FTIR spectroscopy. In these experiments, both catalysts were calcined at 500 °C to form PdO and then reduced to Pd metal at 140 °C in the presence of CO. When the CO-covered catalyst was exposed to CO oxidation reaction conditions at 140 °C, the 2.5% Pd/Al_2O_3 catalyst remained nearly fully reduced, and the surface coverage of CO did not change, indicating irreversible CO adsorption and very low reactivity toward oxygen. On the other hand, the more active 2.5% Pd/La–Al_2O_3 catalyst was more reactive toward oxygen, with a portion of the Pd becoming oxidized when the gas phase was switched from pure CO to the reaction mixture. There was a drop in surface coverage of CO when switching from pure CO to the reaction mixture on the Pd/La–alumina. The results suggest that the role of the La–alumina support is 2-fold, increasing the dispersion of Pd by forming small, stable Pd particles and allowing a portion of the Pd to exhibit facile redox behavior at low temperatures, making the Pd less susceptible to poisoning by CO. This work provides insights into factors that could lead to improved low-temperature CO oxidation reactivity in Pd-based automotive exhaust catalysts.

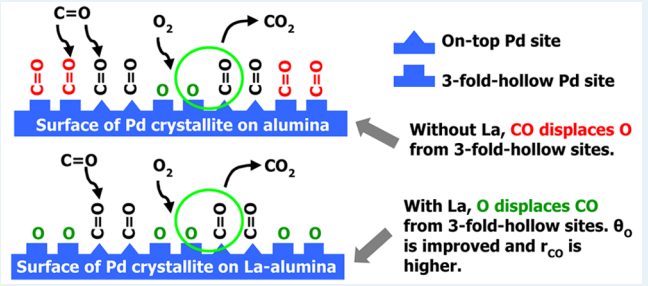

KEYWORDS: *STEM, CO oxidation, DRIFTS, EXAFS, in situ, lanthana-stabilized alumina, palladium, Pd/alumina, XANES*

1. INTRODUCTION

Platinum group metals, particularly Pt and Pd, are critical components in automotive after-treatment applications. Pd is commonly used to oxidize CO and unburned or partially burned hydrocarbons in both stoichiometric (three-way catalyst) and lean burn (diesel oxidation catalyst) engine exhaust. Diesel oxidation catalysts are a particular challenge in terms of materials because diesel exhaust tends to run cooler than gasoline exhaust but is subject to severe exotherms during the regeneration of the diesel particulate filter. Thus, the catalyst must withstand harsh hydrothermal conditions while still performing adequately at low temperature. In diesel applications, Pd is usually paired with Pt because the alloy of these metals is typically more stable and more active than either alone. The high durability demands of these applications have led to many studies of these catalysts under simulated and real-world aging in the hydrothermal conditions of automotive exhaust streams, and the possibility of reducing precious metals cost by developing stable Pd catalysts without Pt has prompted study of the hydrothermal stability of Pd.

We have previously reported on the evolution of metal dispersion on model Pd/Al_2O_3 catalysts during isothermal aging at 900 °C in 10% H_2O/N_2.[1−3] We found that the theta alumina support transformed into alpha alumina during long-term aging, the phase transformation being accelerated by milling of the catalyst during catalyst preparation. The phase transformation to alpha alumina leads to a loss of surface area, but the influence of surface area loss on Pd dispersion was minimal.[3] On the other hand, the Pd supported on the La-stabilized alumina showed the highest dispersion among the catalysts tested. The objective of the present work is to further investigate the role of the La–alumina support on the catalytic reactivity of the Pd using in situ X-ray absorption spectroscopy and FTIR of adsorbed CO.

As a probe reaction, we used the oxidation of CO on Pd, which has been studied extensively beginning in the 1960s by

Received: January 14, 2013
Revised: March 5, 2013
Published: March 8, 2013

Ertl,[4−8] Boudart,[9] and others. A study of reaction intermediates by Engel and Ertl confirmed that the reaction was inhibited by adsorbed CO at low temperatures, with the reaction rate law $r_{CO} = k(O_2)(CO)^{-1}$. Critically, Ertl demonstrated that the simplest mechanistic interpretation of this rate—an Eley−Rideal mechanism of CO striking an oxygen adlayer—was incorrect and that the reaction proceeds via a Langmuir−Hinshelwood mechanism. At low to moderate CO and O_2 coverage, the apparent activation energy is that of the surface reaction; a shift in oxygen adatom geometry at high CO coverage causes this activation energy to decrease from 25 to 14 kcal mol^{-1}. This has been confirmed on Pd clusters on Al_2O_3.[9]

In this study, we are interested in understanding the low-temperature regime for CO oxidation, particularly the evolution of the catalyst under lean conditions. In typical automotive applications, the catalyst that is cooled from high temperatures in a lean mixture will be present entirely as PdO and is reduced only when the vehicle is started for the first time and the catalyst is exposed to reductants such as CO and unburned or partially burned hydrocarbons. This activation process is of significant interest because it determines the lightoff temperature. In our experiments, we started with a fully oxidized catalyst and then exposed it to a stoichiometric reaction mixture. To investigate further the origins of low-temperature reactivity, we switched the catalyst from a stoichiometric reaction mixture to pure CO at 140 °C, where we see significant reactivity in the Pd/La−alumina. These studies help shed light on the influence of the support on the reactivity of Pd for CO oxidation.

Diffuse reflectance infrared Fourier transform spectroscopy (DRIFTS) is a valuable tool for understanding surface species and reaction intermediates on Pd/Al_2O_3 during methane combustion,[10] and CO oxidation.[11,12] EXAFS can be used to determine structural information of small supported metal particles and thus serves as a valuable tool for catalyst characterization of platinum group metals,[13−15] including Pd[16−18] In situ XAS of Pd is capable of observing changes in metallic state during reaction.[15] Frenken et al. have previously utilized in situ XRD and XPS to observe cyclic formation and removal of oxide layers on Pd during CO oxidation.[19,20] The combination of XAS and DRIFTS in this work allows us to observe the catalyst structure, oxidation state, and multiple CO adsorption modes, providing a detailed understanding of the interaction of Pd, O, and CO under reaction conditions.

2. EXPERIMENTAL SECTION

2.1. Synthesis and Characterization. The alumina support was boehmite (DISPAL 23N4-80 alumina, SASOL) that had been calcined in a box furnace at 650 °C for 10 h to transform it to γ-alumina. The La−alumina support (MI-380, W.R. Grace) was used without further modification. Palladium (Sigma Aldrich 4.3 wt % Pd in 10% HNO_3) was deposited on the supports in two aliquots via incipient wetness impregnation. Samples were dried at 120 °C for 2 h after each aliquot addition. After drying for the second time, the samples were calcined in air at 600 °C in a box furnace for 2 h. The reference Pd metal powder was obtained from Sigma Aldrich. Elemental analysis of the materials using energy dispersive X-ray spectroscopy during the scanning transmission electron microscopy experiments (EDS STEM, described in Section 2.4) confirmed each catalyst contained 2.5% Pd and the $Pd/La−Al_2O_3$ catalyst contained 3% La. The BET surface area of each catalyst was measured on a Micromeritics Gemini 2360 using N_2 at 77 K and found to be 150 m^2 g^{-1} for the 2.5 wt % Pd/Al_2O_3 catalyst and 180 m^2 g^{-1} for the $Pd/La−Al_2O_3$ catalyst.

2.2. Reactivity Measurements. CO reactivity was measured using a fresh aliquot of 20 mg of catalyst loaded into a stainless steel tube measuring 1/4 in. with glass wool packed on both sides of the catalyst bed. The products were analyzed using a Varian CP-4900 Micro-GC utilizing a TCD detector. The reactor tube was then mounted inside a high-temperature oven where all pretreatments and reactions were carried out. A thermocouple was inserted in the stainless steel tube reactor touching the catalyst bed, and a second thermocouple was placed in the oven. Gas flow rates were controlled with a mass flow controller, and the catalyst was subjected to an oxidation treatment before reactivity measurements. For the catalyst pretreatment, we used 1% O_2/He at 76 mL min^{-1} with temperature ramped at 10 °C/min/ to 500 °C and held for 1 h. After the oxidation treatment, the sample was cooled back to room temperature and exposed to the reaction mixture at room temperature. The flow rates were 1.5 mL min^{-1} CO, 1 mL min^{-1} O_2, and 75 mL min^{-1} of He, yielding concentrations of 1.9% CO and 1.3% O_2. The effluent composition was recorded every 3 min as the catalyst was heated at 2 °C min^{-1} from 35 to 300 °C. After the first reaction, the sample was cooled in the reaction mixture, and the experiment was conducted a second time to determine the reproducibility of the lightoff curve.

2.3. Simultaneous In Situ X-ray Absorption and Diffuse Reflectance Infrared Spectroscopy. X-ray absorption (XAS) and diffuse reflectance Fourier transform infrared spectroscopy (DRIFTS) experiments were conducted at beamline 9BM of the Advanced Photon Source. A pellet ∼3 mm in diameter and 8 mm long was pressed using approximately 70 mg of catalyst; the top of this pellet was lightly abraded to reduce specular reflection, and this surface was monitored via diffuse reflectance IR spectroscopy. This pellet was loaded into a sample holder within a sealed environmental chamber, which in turn was placed inside a Harrick Scientific Praying Mantis collector of a Bruker Tensor 37 FTIR. The sample holder was equipped with glassy carbon windows to allow an X-ray beam to pass through the sample at a point ∼3 mm below the top surface of the pellet. Gases were introduced into the environmental chamber and were allowed to flow around the pellet in a down flow pattern. A heating element beneath the pellet was used to control the temperature of the catalyst. Helium, 1% O_2/He, and 1% CO/He were delivered using mass flow controllers. X-ray absorption was measured using ionization chambers placed in the beam before and after the sample. DRIFTS measurements, each taken over the course of 3.7 min, were collected continuously. Each 32 min XAS measurement ($E_0 - 300 < E_0 < E_0 + 973$ eV; $E_0 = 24532.6$ eV) was taken 30 min after a change in temperature or gas concentration. Measurements were taken at 25 and 140 °C at a total flow rate of 17 cm^3 min^{-1} consisting of either He, 1% O_2, 1% CO, or 0.6% CO + 0.4% O_2. Analysis of the XAS data was performed using the Demeter software package.[21] The final Pd−Pd coordination numbers of the catalysts, measured via EXAFS at room temperature, were used, along with a slightly modified Pt−Pt size-coordination relationship by de Graaf[22] to estimate Pd particle size for each catalyst after the XAS−DRIFTS experiment.

2.4. Scanning Transmission Electron Microscopy. Electron microscopy was performed on both catalysts after

dx.doi.org/10.1021/cs400024u | ACS Catal. 2013, 3, 846−855

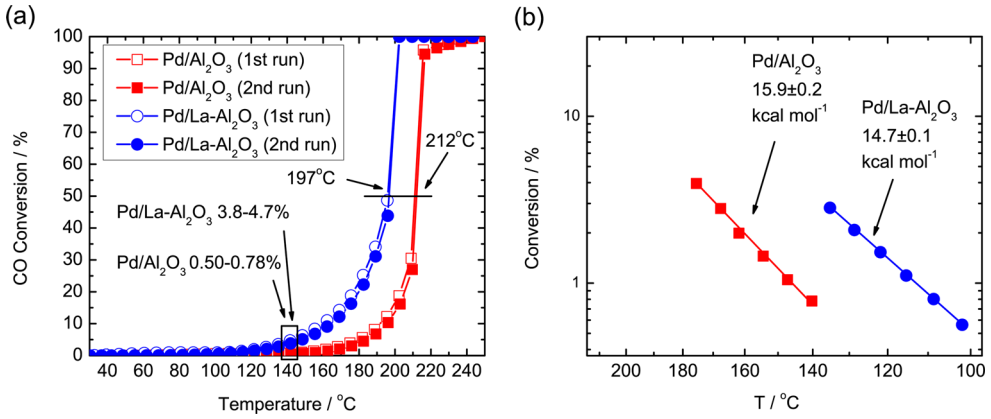

Figure 1. (a) Lightoff traces of 2.5% Pd/La–Al_2O_3 and 2.5% Pd/Al_2O_3 and (b) associated Arrhenius plot. Samples of 20 mg were treated in 75 cm^3 min^{-1} of 1% O_2/He for 1 h at 500 °C and cooled to 30 °C prior to the lightoff ramp from 30 to 250 °C at a rate of 2 °C min^{-1} in 75 cm^3 min^{-1} of 1.9% CO and 1.3% O_2. Repetition of the lightoff trace demonstrated a very small degree of deactivation with respect to the gap in activity between the La-containing and La-free catalysts.

the XAS–DRIFTS experiments using a FEI Titan G2 80–300 kV with a CEOS aberration corrector. The probe size was ~0.8 Å, allowing us to record images of Pd ranging all the way from single atoms to metal clusters and nanoparticles. The catalyst sample was crushed in a mortar with ethanol, and the TEM grid was dipped in this suspension. Prior to STEM imaging, the catalyst sample was subjected to a beam shower to desorb any adsorbed hydrocarbons and prevent sample contamination during imaging. For each catalyst, a particle size distribution was determined, and an atomic-average size distribution was derived for comparison with the EXAFS-derived particle size. These average particle sizes, estimated by both EXAFS and STEM, were subsequently used to determine Pd dispersion, active site content, and CO turnover frequency at 140 °C during the CO lightoff experiment.

3. RESULTS AND DISCUSSION

3.1. Lightoff and Apparent Activation Energy. CO oxidation was performed on the 2.5% Pd/Al_2O_3 and 2.5% Pd/La–Al_2O_3 catalysts in a temperature-programmed mode, and the results show that the catalyst supported on the La–alumina was significantly more active for CO oxidation (Figure 1a). The T_{50} value, or temperature at 50% conversion of CO, is reduced from 212 to 197 °C when La is present. Apparent activation energies (E_A) calculated from these data (Figure 1b) are 16 kcal mol^{-1} for Pd/Al_2O_3 and 15 kcal mol^{-1} for Pd/La–Al_2O_3. Prior work on CO oxidation over Pd has shown E_A is primarily influenced by the surface reaction step, and the activation energy of this surface reaction is influenced by CO and O_2 coverage.[4−6] At low CO coverage, the activation energy is ~25 kcal mol^{-1}, essentially the activation energy of the surface reaction. At moderate CO coverage, the reaction is inhibited by CO blocking O_2 from adsorbing to the surface. Temperature effects on O_2 and CO coverage are such that they essentially negate each other, and the E_A is still that of the surface reaction. With high CO coverage, CO inhibition remains, but oxygen adatoms on Pd shift from a $p(2 \times 2)$ geometry to a more tightly arranged $\sqrt{3} \times \sqrt{3}$ R 30° geometry, which reduces LH activation energy. This results in E_A = 14 kcal mol^{-1} at high CO coverage. This condition may be observed at low temperature and at least parts per million level CO in the gas stream. Although the interdependence of these adsorption kinetics may promote complex oscillatory behavior,[6−8] the investigation of such phenomena is outside the scope of this work. Despite Pd/La–Al_2O_3 being much more reactive than Pd/Al_2O_3, both catalysts have an E_A of 15–16 kcal mol^{-1} below 180 °C and, thus, may proceed by the same LH mechanism under these conditions. We can further infer both catalysts present Pd surfaces with high CO coverage and oxygen adatoms in the compressed $\sqrt{3} \times \sqrt{3}$ R 30° geometry.

We considered the possibility at this stage that the catalysts may initially consist of PdO and that there may be a reaction PdO + CO → Pd + CO_2 occurring, which may have some effect on the lightoff profile. The complete reduction of the catalyst from PdO to Pd under the reaction conditions in Figure 1 would have required 4.7 μmol of CO, or ~14 s of exposure to the gas stream if all CO were consumed. This is a very small contribution to the reactivity under the conditions tested; in Figure 1a, the extremely small discrepancy between the first and second runs of each sample accounts for 24 μmol CO for Pd/Al_2O_3 and 22 μmol CO for Pd/La–Al_2O_3. It is clear that although CO may reduce the catalyst and be consumed in the process, this PdO reduction mechanism is a trivial side process that does not appreciably affect the overall CO oxidation rate. This is consistent with the common assertion that PdO is a poor CO oxidation catalyst.

Average particle sizes for the catalysts were estimated using scanning transmission electron microscopy (STEM) and extended X-ray absorption fine structure (EXAFS) of the catalysts. Using these data, and the conversion of CO at 140 °C in Figure 1, the Pd dispersion, active site concentration, and turnover frequency (TOF) for each catalyst was calculated (Table 1). It is expected that STEM will overestimate particle size because larger particles are more easily observed, and EXAFS will underestimate particle size by capturing lone Pd. Further, Pd oxide particles will reduce the estimated average particle size via EXAFS but may reduce or increase the estimated average particle size via STEM. For this reason, we offer these data, using complementary techniques, only to demonstrate two important trends: that the La increases not only Pd dispersion, but TOF, as well, such that the increased CO oxidation rate with La is caused by factors other than improved dispersion.

3.2. Simultaneous X-ray Absorption Spectroscopy and Infrared Spectroscopy. Investigation of both catalysts was conducted in situ at a reaction temperature of 140 °C,

dx.doi.org/10.1021/cs400024u | ACS Catal. 2013, 3, 846–855

Table 1. Selected Properties of Catalysts Determined via Reactivity Measurement, STEM, and EXAFS[a]

		Pd/Al_2O_3	Pd/La–Al_2O_3
	CO combustion rate (μmol s^{-1} $gcat^{-1}$)	0.077	0.583
STEM	Pd particle size (nm, atomic average)	6.6	4.3
	Pd dispersion (%)	17	26
	Pd active site content (μmol $gcat^{-1}$)	40	61
	TOF (10^{-3} s^{-1})	1.92	9.54
EXAFS	Pd particle size (nm, atomic average)	2.2	1.9
	Pd dispersion (%)	51	59
	Pd active site content (μmol $gcat^{-1}$)	120	138
	TOF (10^{-3} s^{-1})	0.64	4.21

[a]CO combustion rate at 140°C measured during CO lightoff experiment. EXAFS determined at room temperature at end of DRIFTS–XAFS experiment. STEM measurements made after DRIFTS–XAFS experiment.

where we see significant differences between the Pd/alumina and Pd/La–alumina. We used a reaction cell that allowed us to perform simultaneous measurements using X-ray absorption spectroscopy (XAS) and diffuse reflectance infrared Fourier transform spectroscopy (DRIFTS). With this approach, not only Pd–CO surface intermediates (DRIFTS) but also Pd oxidation state and geometry (XAS) could be observed.

Each catalyst was exposed to the set of treatment temperatures and gas environments described in Figure 2. The samples were first heated to 500 °C in flowing 1% O_2 for 30 min to remove contaminants and then cooled to room temperature. The sample was exposed to seven sequential test conditions, which are labeled A through G. Steps A–C, conducted at 25 °C, utilized CO as a probe for reversible and irreversible Pd–CO adsorption sites by beginning with a clean surface (A), applying 1% CO (B), and then purging with He (C). Steps D–F, conducted at 140 °C, were used to observe Pd–CO intermediates and the reduction of Pd by CO, by introducing 0.6% CO and 0.4% O_2 (D), 1% CO (E), and 0.6% CO with 0.4% O_2 again (F). A final measurement at room temperature in 0.6% CO with 0.4% O_2 (G) indicated the final state of the catalyst.

3.2.1. X-ray Absorption near Edge Spectroscopy (XANES). X-ray absorption near edge spectroscopy (XANES) of these samples is shown in Figure 3. The peak at 24 375 eV and trough at 24 405 eV represent PdO, and the weak peak at 24 370 eV and strong peak at 24 395 eV represent Pd metal. The transition of PdO to Pd can be most easily followed by observing the simultaneous decrease of the 24 375 eV PdO peak and increase of the 24 395 eV Pd metal peak. Both catalysts contained PdO after pretreatment (A), and there was no significant degree of reduction of the PdO after CO introduction and purging at 25 °C (B, C). After heating to 140 °C and introduction of CO + O_2 (D), the PdO on the alumina support was partially reduced, and the PdO on the La-containing sample remained in oxide form. With O_2 removed (E), CO almost completely reduced the La-free sample, and subsequent measurements (F, G) indicated further reduction, which may indicate the sample was still being reduced during the XAFS measurement at E. Significantly, this behavior is not seen on the La-containing sample, which did not show any degree of reduction during the CO oxidation reaction, but instead was reduced only when O_2 was removed (E), and this catalyst was partially reoxidized when O_2 was reintroduced (F). Once cooled to 25 °C in the same CO + O_2 mixture, the sample was again reduced (G).

Because the FTIR measured only the top surface of the catalyst pellet, while the XAS measured a portion of the catalyst ~3 mm below the top surface, we must consider the gradient in CO and O_2 concentration as the gas flows down the pellet in the DRIFTS cell during CO oxidation. The specific flow rate for the XAS–DRIFTS measurements was ~0.5 mL min^{-1} $mgcat^{-1}$, or 1/5 of the specific flow rate of the lightoff measurements so that CO conversion at 140 °C during the XAS–DRIFTS experiments would be estimated at 20% for the La-containing catalyst and 2.5% for the catalyst without La. Thus, the largest possible gradient would be that for the La-containing catalyst, in which the inlet stream contained 0.6% CO and 0.4% O_2, and the outlet stream contained an estimated 0.5% CO and 0.3% O_2. As will be shown, the observation of CO_2 bands and partial suppression of CO bands on the La-containing catalyst indicate significant conversion occurred at the surface being probed by FTIR, likely due to circulation of the reactant gas around the catalyst so that the concentration gradient from the FTIR zone to the XAS zone must be significantly less than the maximum possible 20% conversion. Concentration gradients were, of course, negligible at room

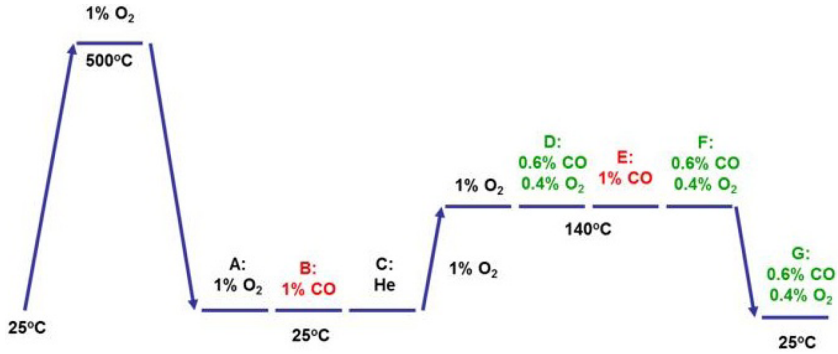

Figure 2. Order of experimental conditions. (A) Catalysts were treated at 500 °C in 1% O_2 for 30 min, then cooled to 25 °C. (B) XAS–DRIFTS were measured as 1% CO was applied and then (C) purged with He. The sample was then heated to 140 °C in 1% O_2 and held in 1% O_2 for 30 min. (D) XAS–DRIFTS was again measured under 0.6% CO and 0.4% O_2, and while O_2 was briefly (E) removed and (F) restored. The sample was then cooled to 25 °C, and a final measurement was taken under CO + O_2. Each segment (A–G) represents 30 min of IR measurement, followed by 30 min of a single XAFS measurement. IR measurements confirmed, in all cases, the stability of surface features when the XAFS measurement was started.

dx.doi.org/10.1021/cs400024u | ACS Catal. 2013, 3, 846–855

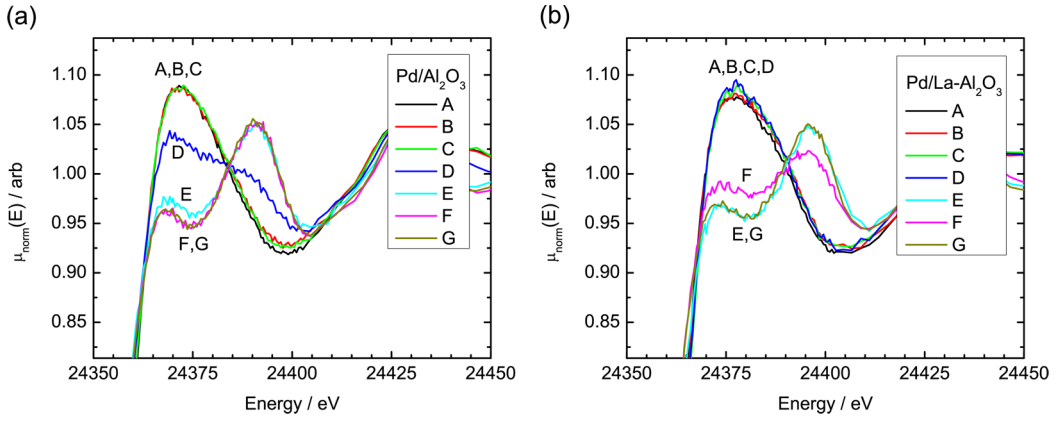

Figure 3. X-ray absorption near edge spectra (XANES) of (a) Pd/Al_2O_3 and (b) $Pd/La–Al_2O_3$.

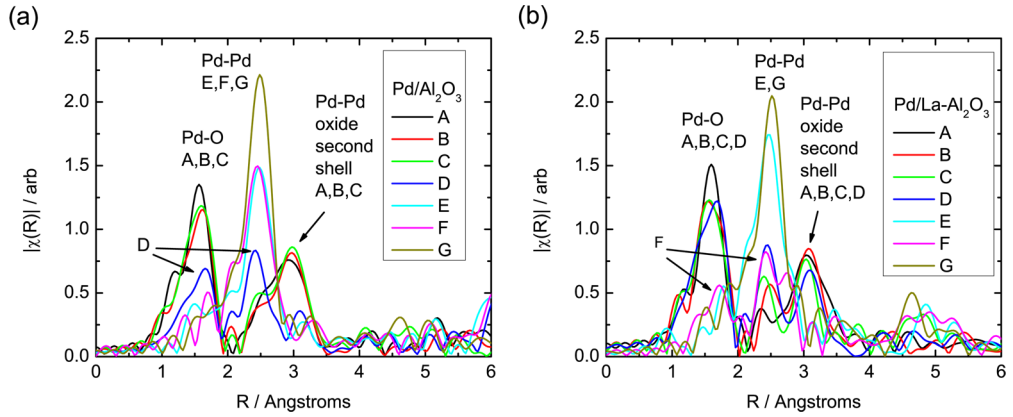

Figure 4. EXAFS of (a) Pd/Al_2O_3 and (b) $Pd/La–Al_2O_3$.

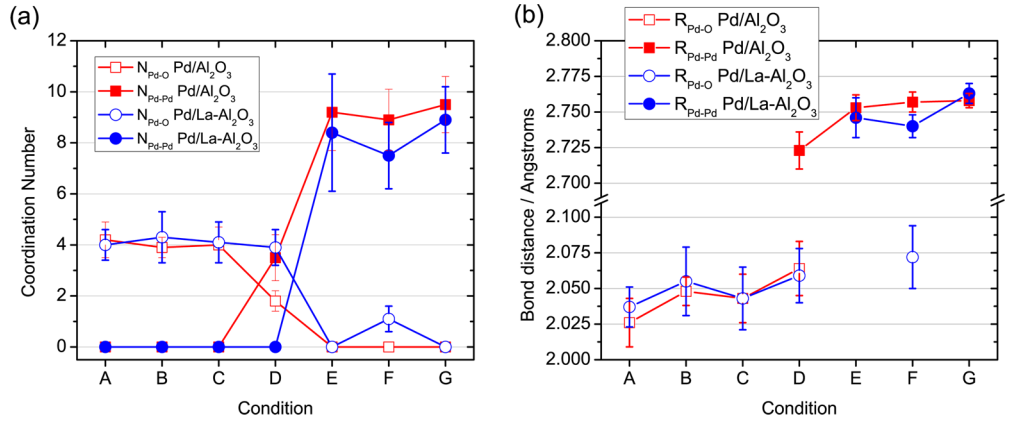

Figure 5. (a) Coordination numbers and (b) bond distances of Pd–O and Pd–Pd paths for 2.5% catalysts as determined by ab initio fitting to the EXAFS spectra in Figure 4. Full tables are available as Supporting Information.

temperature and at 140 °C without O_2, where CO could not be consumed after the catalyst achieved steady state.

3.2.2. Extended X-ray Absorption Fine Structure. EXAFS of the catalysts (Figure 4) showed the initial presence of Pd–O and Pd second-shell paths consistent with PdO for both samples. The weak intensity of the second shell indicated these particles are small. The Pd/Al_2O_3 catalyst was not significantly changed during pretreatments A–C, confirming the same assertion from XANES. Although the $Pd/La–Al_2O_3$ catalyst remained almost entirely PdO over conditions A–C, a weak Pd–Pd metal oscillation appeared upon CO exposure and remained when CO was removed, indicating a very small number of metallic domains. At 140 °C under CO + O_2 (D), a portion of the PdO in the Pd/Al_2O_3 sample became metallic, as seen by the reduction in the Pd–O feature and increase in the Pd–Pd feature. The extent of Pd in metallic form increased when O_2 was removed (E), and Pd remained metallic when O_2 was returned to the catalyst (F). Exposure of the $Pd/La–Al_2O_3$ to CO + O_2 at 140 °C slightly increased the intensity of the Pd–Pd feature, although Pd–O and oxide second-shell features were not affected. When O_2 was removed (E), both Pd–O and oxide second-shell features disappeared, and the Pd–Pd feature became very intense, consistent with the complete or near-complete reduction of PdO to Pd metal. Upon reintroduction

dx.doi.org/10.1021/cs400024u | ACS Catal. 2013, 3, 846–855

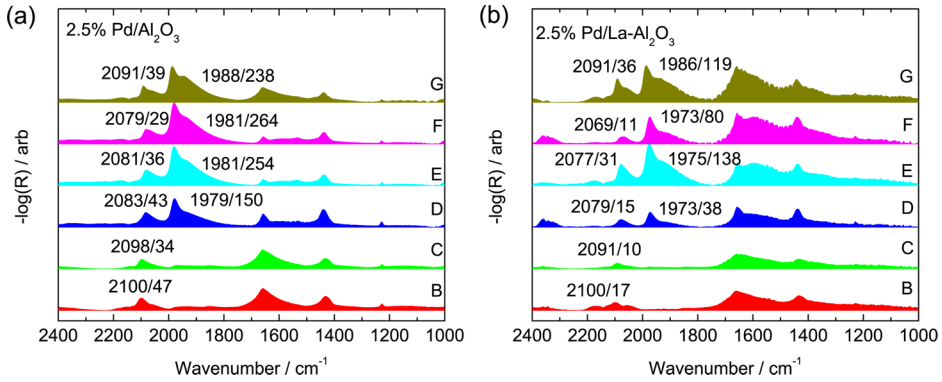

Figure 6. DRIFTS of (a) 2.5% Pd/Al_2O_3 and (b) 2.5% $Pd/La–Al_2O_3$ catalysts after establishment of steady-state conditions. Peak positions (cm^{-1}) and integrated peak area (arb) are identified for the monodentate feature at 2100–2079 cm^{-1} (Pd linear carbonyl) and the multidentate region from 2000 to 1800 cm^{-1} (consisting of a sharp peak at 1988–1973 cm^{-1} attributed to the Pd bridging carbonyl and a wide shoulder extending toward 1800 cm^{-1} attributed to 3-fold hollow species). On the Pd/Al_2O_3 catalyst, for example, at steady state for condition B, there is a linear carbonyl at 2100 cm^{-1} with an intensity of 47 arbitrary units.

of O_2 (F), the height of the Pd–Pd feature decreased to where it was at condition D, and some Pd–O was produced, although the lack of oxide second shell indicated that bulk PdO in condition D was not reformed. This suggests that the reoxidation of Pd at 140 °C on the La–alumina is a surface phenomenon and no bulk PdO is formed at this low temperature.

Coordination numbers and bond distances extracted from the EXAFS data are presented in Figure 5. Both catalysts were initially 4-fold Pd–O (R = 2.03 Å) consistent with PdO, although this may also include the contribution of a dispersed PdO phase present on the alumina surface. Application of CO slightly increased the Pd–O bond distance to 2.05 Å, although this change may be within experimental uncertainty. Although a possible Pd–Pd bond was observed on $Pd/La–Al_2O_3$ in conditions B–D, this feature could not be separated from the oxide second-shell well enough to fit effectively. Upon CO + O_2 application at 140 °C (treatment D), the $Pd/La–Al_2O_3$ catalyst remained 4-fold oxide with a temperature-induced Pd–O shift to R = 2.06 Å, and the Pd/Al_2O_3 catalyst showed an average Pd–O coordination of 2 (R = 2.06 Å) and an average Pd–Pd coordination of 4 (R = 2.73 Å). The Pd/Al_2O_3 catalyst would thus appear to be ∼50% PdO with 4-fold Pd–O coordination and 50% Pd metal nanoparticles with 8-fold Pd–Pd coordination (R = 2.73 Å). When O_2 was removed (E) both catalysts appeared as metal nanoparticles with Pd–Pd coordination around 9 (R = 2.75 Å). When O_2 was reintroduced (F), Pd/Al_2O_3 was not significantly altered, whereas on the $Pd/La–Al_2O_3$ catalyst, Pd–Pd coordination decreased to 7.5 (R = 2.74 Å) and a Pd–O coordination of 1 appeared (R = 2.07 Å). This condition apparently was not favored at lower temperature because cooling to room temperature in CO + O_2 caused Pd to again form metal particles.

As described in Section 3.1, the reduction of PdO with CO has a negligible effect on the reaction rate under these conditions so that the observed reaction rate can be directly correlated to the redox behavior of the Pd metal catalyst. The more active $Pd/La–Al_2O_3$ appears to have a much stronger affinity for oxygen and remains an oxide at 140 °C under CO + O_2. Without O_2, the catalyst is fully reduced whether or not La is present; however, La promotes the recapture of O_2 and subsequent reoxidation of Pd. These processes correlate with more than a 5-fold increase in CO TOF.

Although bulk oxidation of Pd generally does not occur below 400 °C, Pd can adsorb surface oxygen at low temperatures, and this may diffuse into the bulk at temperatures as low as 150 °C.[23] The formation of bulk oxide generally proceeds first through O_2 adsorption, followed by dissolution into the Pd metal, and then PdO crystal growth upon reaching a critical subsurface oxygen content.[24,25] The Pd/Al_2O_3 catalyst under CO + O_2 at 140 °C (condition D) and $Pd/La–Al_2O_3$ catalyst under CO at 140 °C (condition E) had short Pd–Pd bond distances (R = 2.73 Å), which is the opposite of what would be expected for a Pd metal with substantial subsurface oxygen content. This distance was also unusually small for an FCC crystal with average Pd–Pd coordination near 8 but could be explained by a shift from icosahedral (FCC) to octahedral configuration.[26,27] If so, this octahedral structure may be an intermediate phase of Pd between FCC Pd nanoparticles and bulk oxide.

Previous work has suggested that the most active Pd surface is Pd(111) with a layer of chemisorbed oxygen, which was unique in its ability to coadsorb CO.[28] Indeed, the maintenance of an oxygen adlayer appears critical to preventing excessive CO adsorption and inhibition.[29] Evidence indicates a Pd(100) surface may be more active when oxide domains are present.[30] Reversible oxygen storage on supported Pd may be limited to an intermediate size regime because large particles are resistant to oxidation but small particles are irreversibly oxidized.[31−33]

3.2.3. Diffuse Reflectance Infrared Fourier Transform Spectroscopy. Further information on the differences between these catalysts was determined using DRIFTS (Figure 6). After exposure to CO at 25 °C (B), both Pd/Al_2O_3 and $Pd/La–Al_2O_3$ catalysts produced a feature at 2100 cm^{-1} attributed to a linear carbonyl on an oxidized Pd ($Pd_1^{\delta+}$–CO) as well as features at 1655, 1440, and 1230 cm^{-1} associated with adsorption of CO by the alumina support as carbonates and bicarbonates.[11,12,34−37] Very weak gas-phase CO features were observed at 2170 and 2100 cm^{-1}; in general, the lower-wavenumber feature was overwhelmed by Pd linear carbonyls. Beginning with the CO purge in condition C, CO features were consistently 4–10 cm^{-1} lower in wavenumber when La was present.

After CO was purged (C), the $Pd_1^{\delta+}$–CO feature decreased slightly and shifted to 2098 cm^{-1} on alumina and 2091 cm^{-1} on La–alumina due to the dependence of υ(C═O) on CO coverage. Under CO + O_2 at 140 °C (treatment D), the linear

dx.doi.org/10.1021/cs400024u | ACS Catal. 2013, 3, 846–855

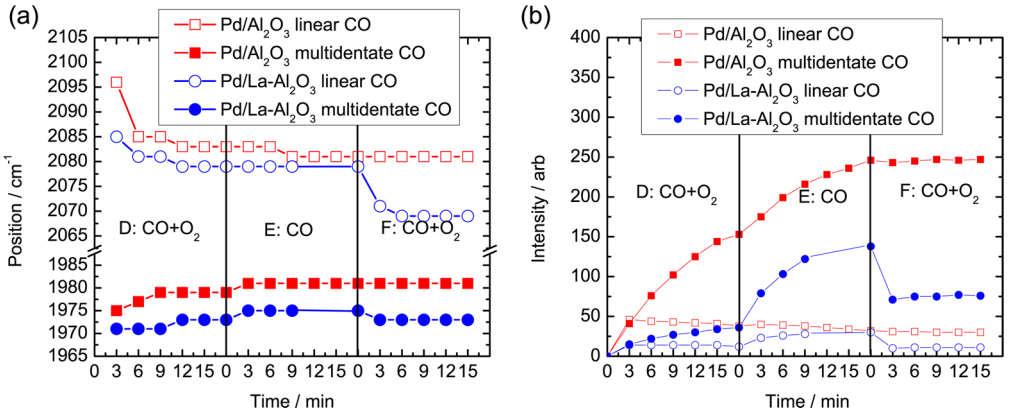

Figure 7. Linear and multidentate CO (a) position and (b) intensity for the Pd/Al_2O_3 and $Pd/La–Al_2O_3$ catalysts over 15 min increments at 140 °C during (D) initial exposure to CO + O_2, (E) removal of O_2, and (F) reapplication of O_2. Spectra used to determine these values are available as Supporting Information.

carbonyl feature further shifted to 2083 cm^{-1} on Pd/Al_2O_3 and 2079 cm^{-1} on $Pd/La–Al_2O_3$, indicating the formation of linear CO on metallic Pd (Pd_1–CO). In addition, a strong bridging carbonyl, Pd_2–CO, is observed at 1979–1973 cm^{-1}, along with a 3-fold hollow Pd_3–CO shoulder. The intensity of these features is much greater on Pd/Al_2O_3 than $Pd/La–Al_2O_3$, which is consistent with $Pd/La–Al_2O_3$ remaining almost entirely oxidized under these conditions and, thus, presenting a very small number of $Pd_{2,3}$ sites. Gas-phase CO_2 was observed on the more active La-containing catalyst as two peaks at 2360 and 2330 cm^{-1}, with some additional structure in the range of 2400–2300 cm^{-1} due to weak interaction with alumina. In addition, a greater degree of bicarbonates are formed on the La-containing catalyst, which form wide bands at 1660 and 1440 cm^{-1}. These species are due to the adsorption of CO_2 formed on Pd subsequently adsorbing to basic hydroxyl sites on the alumina.[34,35]

Upon removal of O_2 (E), where both catalysts were exposed to CO without O_2, the multidentate CO features intensified. Despite both catalysts' having very similar Pd oxidation states and structures, as determined by XAS, as well as similar linear carbonyl coverage, $Pd/La–Al_2O_3$ adsorbed much less CO in 3-fold hollow sites. In addition, once O_2 was reintroduced (F), the 3-fold hollow CO coverage was reduced even further, although not to the intensity before the CO-only step. Conversely, none of the CO was displaced on the Pd/Al_2O_3 catalyst when O_2 was reintroduced. Upon cooling to room temperature (F), the $Pd/La–Al_2O_3$ adsorbed additional multidentate CO. O_2 was therefore displacing Pd_3–CO when La was present, and the amount of displacement was greater at 140 °C than at 25 °C.

Further information regarding CO adsorption modes at 140 °C could be elucidated by observing the evolution of these IR features with time (Figure 7). When exposed to CO + O_2 at 140 °C, both catalysts formed carbonyls within 3 min. Pd_1–CO uptake appeared to be three times higher for the Pd/Al_2O_3 catalyst and appeared at 4 cm^{-1} higher wavenumber, which is indicative of interaction of adjacent carbonyls at high surface coverage. Pd_1–CO sites appeared saturated under CO + O_2, and removal of O_2 did not significantly change either the position or intensity of this feature. At the same time, $Pd_{2,3}$–CO adsorption increased substantially, approaching saturation only after 15 min. Removal of O_2 caused this feature to again increase. This behavior matches the change in oxidation state observed by XANES: CO is reducing PdO, and additional CO is adsorbing on $Pd_{2,3}$–CO as soon as suitable Pd faces appear. These features were unaffected by reapplication of O_2. It is clear, then, that on the alumina support, CO will rapidly adsorb on Pd and inhibit O_2 adsorption.

On the La–alumina, the Pd_1–CO feature was strikingly similar, although much weaker, under condition D owing to the high degree of oxidation of this catalyst. Because this catalyst is so active (conversion is presumably 20% under these conditions), removal of O_2 prevented CO combustion and increased the CO partial pressure above the catalyst; this was reflected in the increase in the carbonyl when O_2 was removed and its decrease when O_2 was returned. The $Pd_{2,3}$–CO feature increased slowly under CO + O_2 (D) and rapidly when O_2 was removed (E). When O_2 was returned (F), nearly half the $Pd_{2,3}$–CO was displaced.

On Pt, CO oxidation involves the surface reaction of Pt–CO linear carbonyls with oxygen adatoms on 3-fold hollow sites.[38] On Pd, there is a greater potential for CO inhibition because of the preferential adsorption of CO on 3-fold hollow sites. At room temperature and below, diatomic oxygen readily adsorbs on Pd (111), much of which dissociates into 3-fold hollow sites, although the heat of adsorption is on the order of −10 kcal/mol.[39] DFT studies of Pd(111) have consistently indicated the adsorption energy of CO on 3-fold hollow sites is on the order of −30 kcal mol^{-1}, 8–12 kcal mol^{-1} lower than on an on-top site.[40]

Clusters on the order of 10 Pd atoms are, through DFT and experimental methods, known to be particularly active for CO oxidation in certain configurations. Monatomic Pd may adsorb multiple CO molecules; this increases the energy barrier of the CO–O bond-forming transition state due to electron withdrawing effects, but the increased energy provided by multiple CO adsorption events nonetheless reduces the apparent activation energy and increases the rate of reaction over a single-CO adsorption path.[41] $Pd_xO_y^+$ cations (x = 4, 5; y = 1, 2) are particularly active for CO oxidation, whereas other configurations are prone to forming stable carbonyls and are thus less active for CO oxidation.[42]

The average coordination number of our La-doped catalyst indicates that the majority of the Pd was not atomically disperse, but was present as Pd particles only slightly smaller than the Pd/alumina. The particle size difference does not adequately explain the significant reduction of 3-fold CO

dx.doi.org/10.1021/cs400024u | ACS Catal. 2013, 3, 846–855

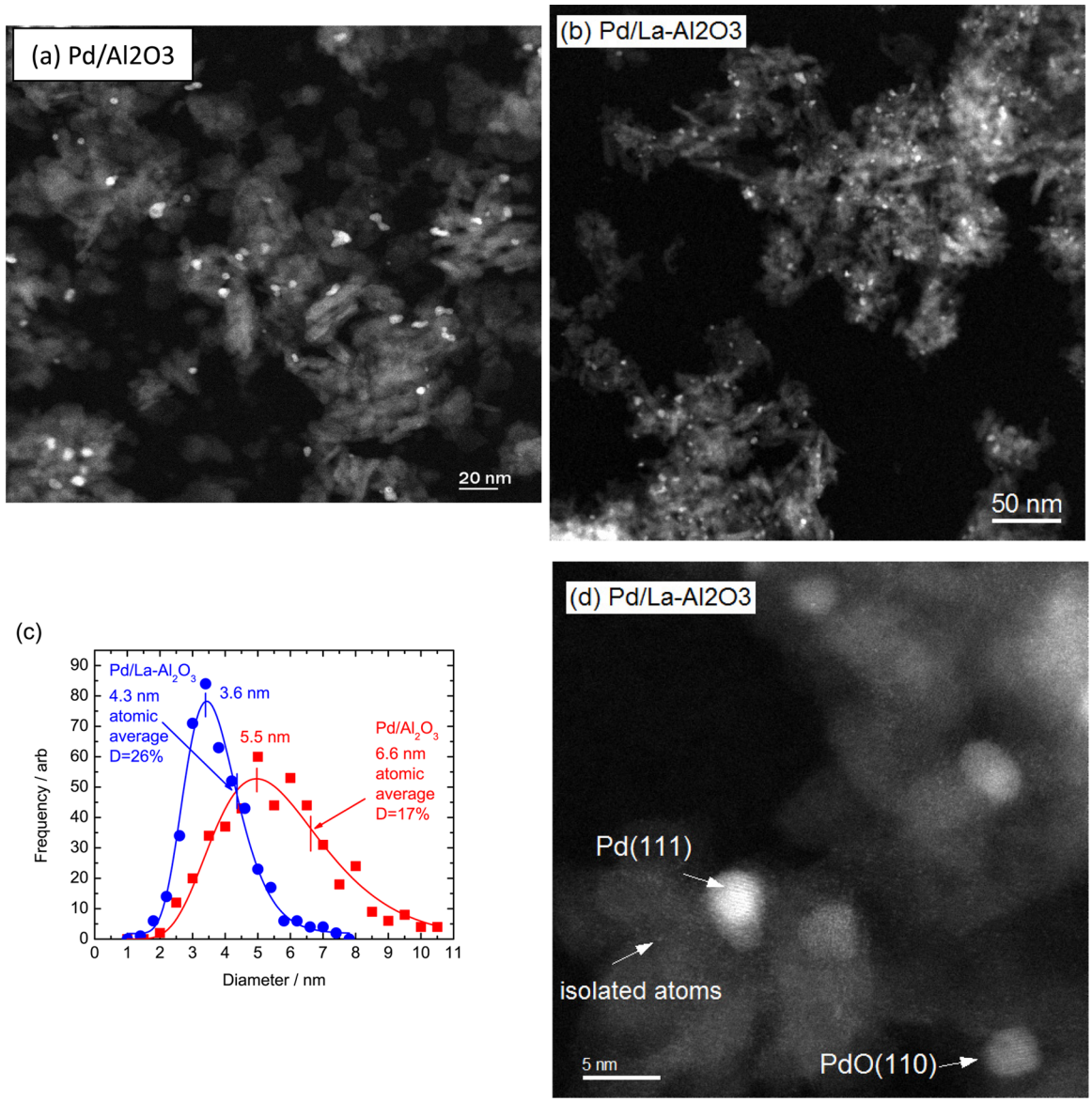

Figure 8. Scanning transmission electron micrographs of (a) Pd/Al_2O_3 and (b) $Pd/La–Al_2O_3$; (c) particle size distribution of Pd in the catalysts, where atomic average particle size is the size of a Pd particle with the same dispersion as the sample; (d) high-resolution STEM of $Pd/La–Al_2O_3$showing lattice images of the Pd nanoparticles and atomically dispersed species on the alumina, which are La and Pd single atoms.

adsorption on the La-doped catalyst; in fact, the similar intensity of the linear carbonyl for both catalysts indicates that these catalysts have extremely similar metallic surface areas. We speculate that there may be something unusual about the metallic faces being exposed by the Pd catalysts when La is present, and this characteristic is responsible for increasing the preference of oxygen adsorption, so much so as to displace CO from 3-fold hollow sites and greatly improve the TOF, but not enough to generate bulk oxide or a passivation layer that would subsequently deactivate the catalyst.

3.3. Scanning Transmission Electron Microscopy. Observation of the catalysts after DRIFTS/XAS testing with aberration-corrected STEM indicates both catalysts contained well-dispersed Pd nanoparticles (Figure 8). Particle counts demonstrated that La decreased the Pd mean particle size from 5.5 to 3.6 nm. A high-resolution image of the La-containing catalyst shows that the air-exposed sample contains significant amounts of PdO and also the coexistence of Pd and PdO in the small particles. This confirms the facile redox behavior of the Pd on La–alumina. The high-magnification STEM image also shows the presence of atomically dispersed species. A careful study of these dispersed species shows they include Pd as well as La atoms. However, since the majority of the Pd in this sample is present in the form of particles >2 nm, we do not expect these dispersed species to make a major contribution. To investigate the reactivity of the dispersed species, we have prepared catalysts with a lower metal loading (0.5 wt % Pd), which show that the dispersed Pd can also be very active for CO oxidation, but only after an oxidative pretreatment at temperatures of 500 °C or greater. The high reactivity of the dispersed Pd species is lost after one CO oxidation cycle, whereas on the catalysts reported here, the reactivity was reproducible, and the second CO oxidation run showed performance similar to the first run. Hence, we conclude that the high reactivity demonstrated on these Pd/alumina catalysts is caused by the presence of small Pd particles stabilized by the La–alumina support.

dx.doi.org/10.1021/cs400024u | ACS Catal. 2013, 3, 846–855

A study by Bueno on Pt/La–Al_2O_3 observed that Pt/La-alumina containing ~3% La consisted of Pt and La well-dispersed on a γ-alumina structure. Reactivity measurements under methane steam reforming indicated that La addition had no effect on activation energy while nonetheless improving TOF. The conclusion was drawn that La aids in the removal of inhibiting C–Pt species.[43] This is similar to our work, in which we conclude La aids in the removal of oxygen-inhibiting $Pd_{2,3}$–CO species. An increase in La $3d_{5/2}$ binding energy and decrease in Pd $4d_{5/2}$ binding energy with increasing La content made a strong case that this promotional effect is highly electronic in nature,[43] which we likewise conclude for Pd via XANES.

The addition of ceria or ceria–zirconia, typical oxygen storage materials utilized in three-way catalysts for gasoline applications, have also been studied. La and Ce have been observed to influence the oxidation state of Pt on alumina under simulated gasoline exhaust conditions. In situ FTIR by Yentekakis observed that species adsorbed to Pt were consistent with Pd^0 with La, Ce doping, and $Pd^{\delta+}$ without.[44] This type of metal-support interaction was determined to be the cause of significant improvement in Pt dispersion for mixed oxide supported catalysts and improved performance under three way catalyst conditions[45] and N_2O reduction conditions.[46]

4. CONCLUSIONS

On the La–alumina, Pd demonstrates a dynamic morphology, exhibiting substantial and generally reversible bulk structure changes in response to lean and rich feed. These particles are generally smaller. Critically, the Pd in these samples is capable of rejecting CO in favor of O_2 in 3-fold Pd sites in the presence of both CO and O_2, whereas on Pd/alumina, these sites exhibit high CO coverage under the same conditions and are thus self-poisoned. We believe that atomically dispersed La species help to modify the nucleation of Pd on the alumina surface, and the smaller clusters that form on the La–alumina behave differently from the larger particles formed on the alumina support. On the La–alumina, these Pd particles show facile transformation into PdO, which can provide an oxygen reservoir for the active metallic region, and that this is a major factor in the improved low temperature performance of Pd/La–Al_2O_3 catalysts that persists at higher temperatures.

■ ASSOCIATED CONTENT

Ⓢ Supporting Information

DRIFTS transients of the catalysts under CO and CO, O_2 at 140 °C, as well as detailed tables of EXAFS regression parameters. This material is available free of charge via the Internet at http://pubs.acs.org.

■ AUTHOR INFORMATION

Corresponding Author

*E-mail: datye@unm.edu.

Present Address

§Present address: Department of Chemical Engineering, University of Michigan, 3074 Herbert H. Dow Building, 2300 Hayward, Ann Arbor, MI 48109-2136 USA. E-mail: jrgaudet@umich.edu.

Notes

The authors declare no competing financial interest.

■ ACKNOWLEDGMENTS

Portions of this work were conducted at beamline 9-BM (CMC) of the Advanced Photon Source, Argonne National Laboratory. Work at the CMC Beamlines is supported in part by the Office of Basic Energy Sciences of the U.S. Dept. of Energy (DOE) and by the National Science Foundation Division of Materials Research. Use of the Advanced Photon Source is supported by the Office of Basic Energy Sciences of the U.S. DOE under Contract No. W-31-109-Eng-38. We gratefully acknowledge funding for this work provided by the U.S. DOE, Office of Science Grant DE-FG02-05ER15712. STEM imaging was performed at the Environmental Molecular Sciences Laboratory (EMSL), a user facility operated by the DOE at Pacific Northwest National Laboratories.

■ REFERENCES

(1) Pham, H. N.; Pagan-Torres, Y. J.; Serrano-Ruiz, J. C.; Wang, D.; Dumesic, J. A.; Datye, A. K. *Appl. Catal., A* **2011**, *397*, 153–162.
(2) Xu, Q.; Kharas, K. C.; Croley, B. J.; Datye, A. K. *ChemCatChem* **2011**, *3*, 1004–1014.
(3) Xu, Q.; Kharas, K.; Croley, B.; Datye, A. *Top. Catal.* **2012**, *55*, 78–83.
(4) Engel, T.; Ertl, G. *Adv. Catal.* **1979**, *28*, 1–78.
(5) Engel, T.; Ertl, G. *J. Chem. Phys.* **1978**, *69*, 1267–1281.
(6) Ertl, G. *Science* **1991**, *254*, 1750–1755.
(7) Zambelli, T.; Wintterlin, J.; Trost, J.; Ertl, G. *Science* **1996**, *273*, 1688–1690.
(8) Bowker, M. *ACS Nano* **2007**, *1*, 253–257.
(9) Ladas, S.; Poppa, H.; Boudart, M. *Surf. Sci.* **1981**, *102*, 151–171.
(10) Demoulin, O.; Navez, M.; Ruiz, P. *Appl. Catal., A* **2005**, *295*, 59–70.
(11) Skotak, M.; Karpiński, Z.; Juszczyk, W.; Pielaszek, J.; Kepiński, L.; Kazachkin, D.; Kovalchuk, V.; d'Itri, J. *J. Catal.* **2004**, *227*, 11–25.
(12) Busca, G.; Finocchio, E.; Escribano, V. S. *Appl. Catal., B* **2012**, *113–114*, 172–179.
(13) van Zon, J. B. A. D.; Koningsberger, D. C.; van't Blik, H. F. J.; Sayers, D. E. *J. Chem. Phys.* **1985**, *82*, 5742–5754.
(14) Kip, B.; Duivenvoorden, F.; Koningsberger, D.; Prins, R. *J. Catal.* **1987**, *105*, 26–38.
(15) Singh, J.; Lamberti, C.; van Bokhoven, J. A. *Chem. Soc. Rev.* **2010**, *39*, 4754–4766.
(16) Matsui, T.; Harada, M.; Bando, K. K.; Toba, M.; Yoshimura, Y. *Appl. Catal., A* **2005**, *290*, 73–80.
(17) Matsui, T.; Harada, M.; Ichihashi, Y.; Bando, K. K.; Matsubayashi, N.; Toba, M.; Yoshimura, Y. *Appl. Catal., A* **2005**, *286*, 249–257.
(18) Cheng, D.; Okumura, K.; Xie, Y.; Liu, C.-j. *Appl. Surf. Sci.* **2007**, *254*, 1506–1510.
(19) Hendriksen, B. L. M.; Ackermann, M. D.; van Rijn, R.; Stoltz, D.; Popa, I.; Balmes, O.; Resta, A.; Wermeille, D.; Felici, R.; Ferrer, S.; Frenken, J. W. M. *Nat. Chem.* **2010**, *2*, 730–734.
(20) Balmes, O.; Resta, A.; Wermeille, D.; Felici, R.; Messing, M. E.; Deppert, K.; Liu, Z.; Grass, M. E.; Bluhm, H.; van Rijn, R.; Frenken, J. W. M.; Westerstrom, R.; Blomberg, S.; Gustafson, J.; Andersen, J. N.; Lundgren, E. *Phys. Chem. Chem. Phys.* **2012**, *14*, 4796–4801.
(21) Ravel, B.; Newville, M. *J. Synchrotron Radiat.* **2005**, *12*, 537–541.
(22) de Graaf, J.; van Dillen, A. J.; de Jong, K. P.; Koningsberger, D. C. *J. Catal.* **2001**, *203*, 307–321.
(23) Nagarajan, S.; Thirunavukkarasu, K.; Gopinath, C. S. *J. Phys. Chem. C* **2009**, *113*, 7385–7397.
(24) Han, J.; Zemlyanov, D. Y.; Ribeiro, F. H. *Surf. Sci.* **2006**, *600*, 2752–2761.
(25) Han, J.; Zemlyanov, D. Y.; Ribeiro, F. H. *Surf. Sci.* **2006**, *600*, 2730–2744.
(26) Kruger, S.; Vent, S.; Nortemann, F.; Staufer, M.; Rosch, N. *J. Chem. Phys.* **2001**, *115*, 2082–2087.

(27) Yudanov, I. V.; Sahnoun, R.; Neyman, K. M.; Rosch, N. *J. Chem. Phys.* **2002**, *117*, 9887−9896.
(28) Gabasch, H.; Knop-Gericke, A.; Schlogl, R.; Borasio, M.; Weilach, C.; Rupprechter, G.; Penner, S.; Jenewein, B.; Hayek, K.; Klotzer, B. *Phys. Chem. Chem. Phys.* **2007**, *9*, 533−540.
(29) Chen, M. S.; Cai, Y.; Yan, Z.; Gath, K. K.; Axnanda, S.; Goodman, D. W. *Surf. Sci.* **2007**, *601*, 5326−5331.
(30) Gerrard, A. L.; Weaver, J. F. *J. Chem. Phys.* **2005**, *123*, 224703−17.
(31) Brandt, B.; Schalow, T.; Laurin, M.; Schauermann, S.; Libuda, J.; Freund, H.-J. *J. Phys. Chem. C* **2007**, *111*, 938−949.
(32) Schalow, T.; Laurin, M.; Brandt, B.; Schauermann, S.; Guimond, S.; Kuhlenbeck, H.; Starr, D. E.; Shaikhutdinov, S. K.; Libuda, J.; Freund, H.-J. *Angew. Chem., Int. Ed.* **2005**, *44*, 7601−7605.
(33) Schalow, T.; Brandt, B.; Starr, D. E.; Laurin, M.; Shaikhutdinov, S. K.; Schauermann, S.; Libuda, J.; Freund, H.-J. *Angew. Chem., Int. Ed.* **2006**, *45*, 3693−3697.
(34) Liu, J.; Ying, P.; Xin, Q.; Li, C. *Appl. Spectrosc.* **1999**, *53*, 40−42.
(35) Rege, S. U.; Yang, R. T. *Chem. Eng. Sci.* **2001**, *56*, 3781−3796.
(36) Sica, A. M.; Gigola, C. E. *Appl. Catal., A* **2003**, *239*, 121−139.
(37) Xu, J.; Ouyang, L.; Mao, W.; Yang, X.-J.; Xu, X.-C.; Su, J.-J.; Zhuang, T.-Z.; Li, H.; Han, Y.-F. *ACS Catal.* **2012**, *2*, 261−269.
(38) Allian, A. D.; Takanabe, K.; Fujdala, K. L.; Hao, X.; Truex, T. J.; Cai, J.; Buda, C.; Neurock, M.; Iglesia, E. *J. Am. Chem. Soc.* **2011**, *133*, 4498−4517.
(39) Guo, X.; Hoffman, A.; Yates, J. T. *J. Chem. Phys.* **1989**, *90*, 5787−5792.
(40) German, E. D.; Sheintuch, M. *J. Phys. Chem. C* **2008**, *112*, 14377−14384.
(41) Reber, A. C.; Khanna, S. N.; Tyo, E. C.; Harmon, C. L.; Castleman, A. W. *J. Chem. Phys.* **2011**, *135*, 234303−7.
(42) Lang, S. M.; Schnabel, T.; Bernhardt, T. M. *Phys. Chem. Chem. Phys.* **2012**, *14*, 9364−9370.
(43) Araujo, J. C. S.; Zanchet, D.; Rinaldi, R.; Schuchardt, U.; Hori, C. E.; Fierro, J. L. G.; Bueno, J. M. C. *Appl. Catal., B* **2008**, *84*, 552−562.
(44) Matsouka, V.; Konsolakis, M.; Lambert, R. M.; Yentekakis, I. V. *Appl. Catal., B* **2008**, *84*, 715−722.
(45) Papavasiliou, A.; Tsetsekou, A.; Matsouka, V.; Konsolakis, M.; Yentekakis, I. V. *Appl. Catal., A* **2010**, *382*, 73−84.
(46) Konsolakis, M.; Drosou, C.; Yentekakis, I. V. *Appl. Catal., B* **2012**, *123−124*, 405−413.